ChemPhysChem

Research Article
doi.org/10.1002/cphc.202200377

Chemistry Europe
European Chemical Societies Publishing

www.chemphyschem.org

Diastereoselectivity on Intramolecular Alder-ene Reaction of 1,6-Dienes

Abel de Cózar*[a, b]

A detailed computational study of the intramolecular Alder-ene reaction of different 1,6-dienes at M06-2X(PCM)/TZ2P level of theory has been performed. We want to understand the influence of enophile-geminal substitution pattern in the *cis*:*trans* selectivity of the cyclization process. Our analysis of the reaction coordinate by means of activation strain model of chemical reactivity (ASM-distortion interaction model) reveals that the *cis*-selectivity observed for unactivated reagents is related with high stabilizing orbital interaction and lower strain energy, consequence of an early transition structure. On the other hand, the presence of activating groups increases the asynchronicity of the transition structures and reduces the activation barrier due to more stabilizing orbital and electrostatic interactions, favoring *trans*-selectivity.

Introduction

The Alder-ene reaction, discovered by Alder in 1943,[1] involves the thermal addition of an electron deficient multiple bond (enophile) to an olefin bearing an allylic hydrogen (ene) to form a C–C bond with the concomitant migration of the ene double bond and 1,5-hydrogen shift (Figure 1C). In this reaction, three stereogenic centers are generated in a single synthetic step. Moreover, due to its simplicity and applicability to a wide range of substituents, Alder-ene reaction has been widely used for the synthesis of complex polycyclic organic structures[2] and has been object of some theoretical studies.[3] Within the Woodward–Hoffmann symmetry rules framework, the Alder-ene reaction can be described as group transfer pericyclic [$_{\pi}2_{s}+{}_{\pi}2_{s}+{}_{\sigma}2_{s}$] 6 electron *supra-supra* facial concerted reaction,[4] symmetry-allowed under thermal conditions, that resembles the Diels–Alder (Figure 1A) and [1,5] sigmatropic shift reactions (Figure 1B) i.e. featuring an aromatic six membered transition state.

Alder-ene reactions are usually associated with relatively high activation barriers, thus requiring harsh reaction conditions, or the presence of activated reagents and/or catalysts.[3e] Theoretical calculations reported by Fernandez and Bickelhaupt[3c] indicate a correlation between the synchronicity of the transition structures and the activation barriers where low activation barriers are associated with asynchronous transition structures in which the C–C forming bond develops earlier than the C–H bond. According to their activation strain (ASM) – distortion/interaction analysis[5] the high activation barriers stems from the activation strain curve. In particular, the lowering barrier effect directly translates from a reduction of

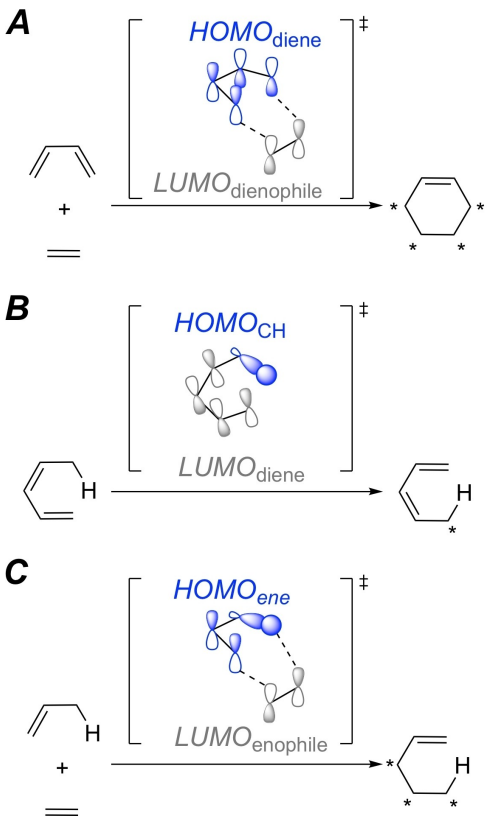

Figure 1. General reaction schemes of (A) Diels–Alder (B) [1,5] sigmatropic H-shift and (C) Alder-ene reactions including schematic representation of main FMO involved. The stereogenic centers created in each reaction type are indicated with an asterisk.

[a] *Dr. A. de Cózar*
Departamento de Química Orgánica I, Facultad de Química, Universidad del País Vasco and Donostia International Physics Center (DIPC) P. K. 1072, 20018, San Sebastián-Donostia, Spain
E-mail: abel.decozar@ehu.eus
Homepage: www.adecozar.com
[b] *Dr. A. de Cózar*
IKERBASQUE, Basque Foundation for Science, Plaza Euskadi 5, 48009 Bilbao, Spain

Supporting information for this article is available on the WWW under https://doi.org/10.1002/cphc.202200377

the ene-reagent strain due to a low overlap between the C–H bond of the hydrogen transferred and the enophile LUMO (i.e. $HOMO_{ene}$–$LUMO_{enophile}$ overlap).[3c]

In particular, intramolecular Alder-ene reaction of dienes offers a valuable method for the synthesis of (hetero)cycles, benefiting from entropic advantages. As a general rule, 1,6-dienes preferentially generate *cis*-five membered rings, whereas 1,7-dienes yields *trans*-six membered rings.[6] Remarkably, the stereochemistry about the forming C–C bond and its relationship with the substitution pattern of the initial reagent is not easy to predict, and can be affected by the presence of activating groups.[6] For example, in the early work of Eros et al.[7] described that the pyrolysis of 7-Methyl-1,6-octadiene (**1a**) at 457 °C yields the exclusive formation of cyclopentene *cis*-**2a** through intramolecular Alder-ene reaction (Scheme 1). On contrary, few years later, the Sarkar et al.[8] reported that presence of CO_2Me on the enophile moiety implies both a rate enhancement (higher overall yields), and an increase of the *trans*-cyclopentene formation. In fact, when malonate derivative **1d** was used, cyclopentane *trans*-**2d** was found as major product (Scheme 1), thus showing the strong relationship between the reagent structure and the *cis*:trans ratio of the product.

However, despite the synthetic usefulness of intramolecular Alder-ene reactions, extensively exploited experimentally,[9] the number of theoretical studies devoted to its understanding is somehow scarce. In an early work of Houk et al.[10] the authors developed a force field based on the rigid transition structure approximation, capable to theoretically simulate the *cis* preference observed in the intramolecular Alder-ene cyclization of unactivated 1,6-dienes. In this work, the authors propose that the diastereoselectivity was associated with a lower deformation of the parent transition structure upon substitution of the tether for the *cis*-transition structure, compared to the *trans*-counterparts. Unfortunately, the developed method does not fit with the experimental evidences when activated 1,6-dienes were considered due to deformations in the transition structure geometry. In 1999, Das[11] re-evaluated the Alder-ene reaction of 1,6-dienes at semiempirical level of theory. In that case, the reported AM1 calculations overestimate the *trans*-product formation of activated 1,6-dienes, whereas provides less accurate *cis*:*trans* ratios than the force field developed by Houk[7] for unactivated 1,6-dienes. In more recent works, the same authors described some discrepancies between *cis*:*trans* theoretical ratios computed at B3LYP/6-31G*//HF/6-31G* and experimental evidences.[12]

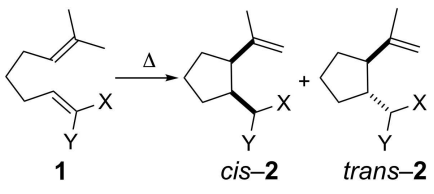

	cis:*trans* ratio
a : X = Y = H	**100**:0
b : X = CO_2Me; Y = H	**76**:24
c : X = H; Y = CO_2Me	43:57
d : X = Y = CO_2Me	13:**87**

Scheme 1. *Cis*:*trans* ratio observed for the intramolecular Alder-ene reaction of 1,6-octadienes. Values taken from Refs. [7,8].

The calculations here presented are focused on the study of the intramolecular ene-Alder reaction of 1,6-dienes and how different substituents affect the *cis*:*trans* diastereoselectivity. Our main objective is to understand if the selectivity changes are consequence of electronic effects, due to the presence of electronwithdrawing groups, or on the other hand, it is a strain-biased process where the presence of substituents drastically affects the geometry of the transition structure, thus the activation energy of the process. To this end, we have quantum-chemically analyzed the reaction profile associated with model reactions to asseses the reliability of the computational chosen method, and later on, we expanded our study to predict *cis*:*trans* ratios of intramolecular ene-Alder reactions not reported in literature. The trends in reactivity were further analyzed by means of the activation strain model of chemical reactivity (ASM-distortion/interaction model).

Computational Details

Theoretical calculations have been carried out within the DFT framework[13] at the M06-2X(PCM)/TZVP level by using the GAUSSIAN 16[14] and AMS2021[15] suite of programs. We have chosen the highly parameterized functional M06-2X[16] in combination with triple-zeta Ahlrichs basis set TZVP[17] due to its suitability for the treatment of nonbonding interactions and dispersion forces.[16] Thermal Gibbs corrections were computed at the same level, at the indicated temperature, and were not scaled. Solvent effects were estimated by the polarization continuum model[18] (PCM) method within the self-consistent reaction field (SCRF) approach.[19] All SCRF-PCM calculations were performed using p-xylene ($\varepsilon = 2.2705$) as model solvent.

All the stationary points were characterized by harmonic vibrational analysis, where local minima showed positive definite Hessians. Fully optimized transition structures showed only one imaginary frequency associated with nuclear motion along the chemical transformation under study. Reaction paths were computed by intrinsic reaction coordinates (IRC) calculations.

Reaction profiles were analyzed using the activation strain (ASM) – distortion/interaction model[5] developed by Bickelhaupt–Houk, modified to unimolecular reactions,[20] including solvation effects.[21] Within this framework, we used ene and enophile fragments calculated in the electronic doublet state with the unpaired electron in a σ orbital to depict the reactant as a "very strongly bound reactant complex".[19] In the selected systems, only two possible fragmentations that do not affect the atoms directly involved in the ene-Alder reaction can be envisaged, namely C3–C4 or C4–C5 bond cleavage. In this study, the C3–C4 bond cleavage was chosen in order to have fragments with similar size (Figure 2). Remarkably, similar results were obtained when C4–C5 fragmentation was selected (See Supporting Information).

The computed solution-phase energy profile $\Delta E_{solution}(\zeta)$ is decomposed along the reaction coordinate ζ into the energy of the solute $\Delta E_{solute}(\zeta)$, the reaction system in vacuum but with its geometry in solution, plus the solvation energy $\Delta E_{solvation}(\zeta)$:

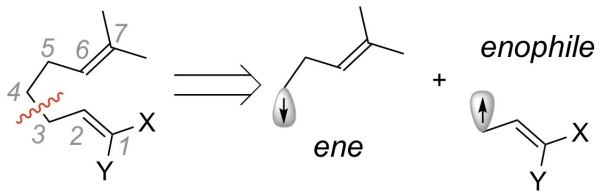

Figure 2. C3–C4 fragmentation of the unimolecular reaction system.

$$\Delta E_{solution}(\zeta) = \Delta E_{solute}(\zeta) + \Delta E_{solvation}(\zeta) \quad (1)$$

In the present work, the reaction coordinate ζ is projected onto the newly formed C–C bond. ($\Delta E_{solvation}(\zeta)$) accounts for both the interaction of the solute with the solvent and the cavitation energy.

The solute energy $\Delta E_{solute}(\zeta)$ is further decomposed as:

$$\Delta E_{solute}(\zeta) = \Delta E_{strain}(\zeta) + \Delta E_{int}(\zeta) \quad (2)$$

where $\Delta E_{strain}(\zeta)$ and $\Delta E_{int}(\zeta)$ correspond to the strain and interaction energy, respectively. The strain energy is associated with the energy required to deform the reactants from their equilibrium geometry to the geometry they adopt along the reaction coordinate ζ. This term is dependent of reactants the rigidity and, in general, is positive (destabilizing) giving rise to the occurrence of the reaction barrier. On the other hand, the interaction term $\Delta E_{int}(\zeta)$ depends on the electronic structure of the reagents and on how they approach each other. This latter term can be further analyzed within the Kohn–Sham MO conceptual framework according to the canonical energy decomposition analysis (EDA)[22] as:

$$\Delta E_{int}(\zeta) = \Delta V_{elstat}\ (\zeta) + \Delta E_{Pauli}(\zeta) + \Delta E_{oi}(\zeta) \quad (3)$$

ΔV_{elstat} is the classical Coulombic interaction between the unperturbed charge distributions of each of the two reactants. ΔE_{Pauli} is the Pauli repulsions between occupied orbitals of the two fragments and is responsible for steric repulsion. ΔE_{oi} stands for the stabilizing orbital interaction energy, including charge transfer.

Cis:*trans* selectivities have been computed by using the Eyring–Polanyi equation[23] from the previously computed Gibbs free activation energies ($\Delta G^{\pm}$), applying Curtin–Hammett kinetics (i.e. the product ratio depends on energy differences of the corresponding TSs) by using equation (4) and imposing the normalization conditions of equation (5):

$$\frac{[cis]}{[trans]} = e^{-\left(\Delta\Delta G^{\pm}/RT\right)} \quad (4)$$

$$[cis] + [trans] = 100 \quad (5)$$

where $\Delta\Delta G^{\pm}$ is the difference between the activation Gibbs free energies and R is the gas constant.

Results and Discussion

Activation and reaction Gibbs free energies as well as the main geometrical features of the transition structures computed at the M06-2X(PCM)/TZVP level of theory associated with the intramolecular ene-Alder reaction of 1,6-dienes **1 a**–**g** are shown in Table 1 and Figure 3, respectively.

Table 1. Activation ($\Delta G^{\pm}$) and reaction (ΔG_{rxn}) Gibbs free energies (in kcal mol^{-1}) of intramolecular ene-Alder reactions computed at M06-2X(PCM)/TZVP level. Thermal corrections were computed at the selected temperature. Theoretical and experimental *cis*:*trans* ratios are also included.

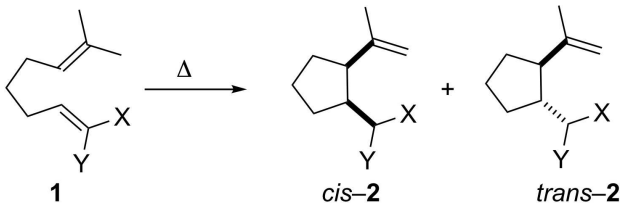

entry		X	Y	2	T/K	$\Delta G^{\pm}$	ΔG_{rxn}	*cis*:*trans*	
								Theor.	Exp.
1	**1 a**	*H*	*H*	*cis*	457	39.1	−11.6	96:4	100:0[a]
2				*trans*		41.9	−13.6		
3	**1 b**	*CO_2Me*	*H*	*cis*	528	37.2	−7.3	66:34	76:24[b]
4				*trans*		37.8	−9.2		
5	**1 c**	*H*	*CO_2Me*	*cis*	528	38.2	−6.5	25:75	43:57[b]
6				*trans*		36.7	−9.1		
7	**1 d**	*CO_2Me*	*CO_2Me*	*cis*	528	38.8	−6.0	2:98	13:87[b]
8				*trans*		31.7	−8.7		
9	**1 e**	*Me*	*Me*	*cis*	298	41.2	−5.7	88:12	–
10				*trans*		42.6	−9.9		
11	**1 f**	*CO_2Me*	*Me*	*cis*	298	37.9	−4.5	4:96	–
12				*trans*		36.0	−7.9		
13	**1 g**	*Me*	*CO_2Me*	*cis*	298	37.5	−6.9	17:83	–
14				*trans*		36.5	−9.9		

[a] Values taken from Ref. [7]. [b] Values taken from Ref. [8].

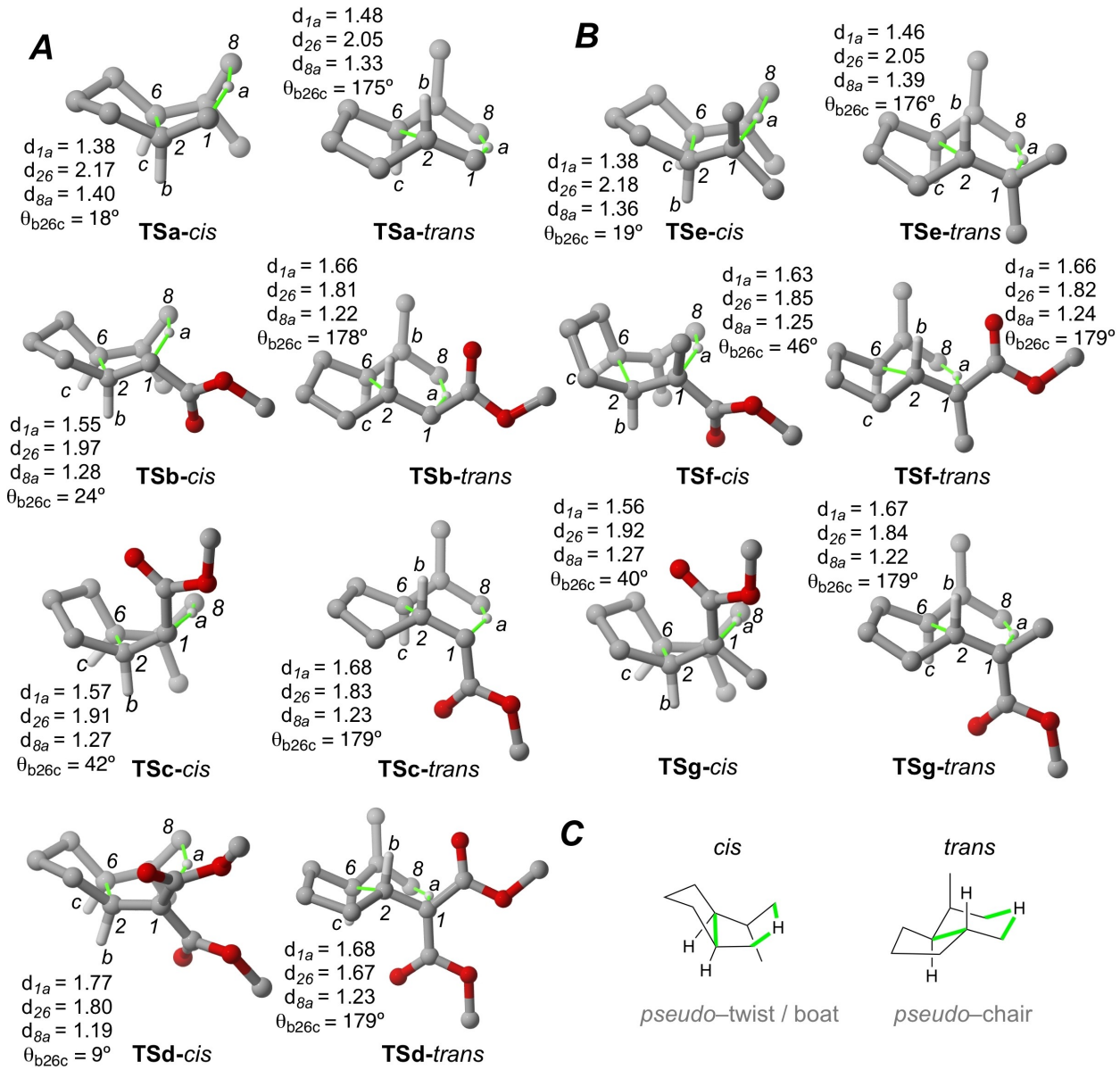

Figure 3. (A, B) Main geometrical features of transition structures associated with the intramolecular ene-Alder reaction of selected 1,6-dienes computed at M06-2X(PCM)/TZVP level. (C) Schematic representation of the *cis*- and *trans*-transition structure geometries. Non-relevant hydrogen atoms are omitted for clarity. Distances are in Å. Angles are in deg.

Our results show that the intramolecular ene-Alder requires harsh conditions, as reflected by the high activation Gibbs barriers computed ($\Delta G^{\ddagger}$). Moreover, the theoretical *cis*:*trans* ratios are qualitatively in good agreement with the values described experimentally,[7,8] thus pointing out the reliability of the selected computational method. In all cases, formation of *trans*-**2a**–**g** is thermodynamically favored as shown by the ΔG_{rxn} values. Therefore, the *cis*-preference observed for compounds **1a**,**b**,**e** can be related to a kinetically favored process, associated with lower activation Gibbs barrier than its *trans*-counterparts rather than a higher stability of the products.[10]

Detailed inspection of the transition structure shows that in all cases, the reaction corresponds to a concerted but asynchronous process where the C2–C6 bond formation develops earlier than the C1-Ha bond breaking/forming process. This asynchronicity is more pronounced for *trans*-transition structures, where the C2–C6 distance d_{26} is 0.03–0.12 Å shorter than their *cis*-counterparts (Figure 3). For activated reagents (X, Y = CO_2Me), we find a relationship between the synchronicity and the activation barrier as described for the bimolecular ene-Alder reaction.[3c] However, unactivated reagents do not follow this trend i.e. transition structure **TS1a**-*trans* is more asynchronous than **TS1a**-*cis*, but the former is less energetically stable. Moreover, we observed that the conformation of the cyclic six-membered transition structure strongly depends on the relative conformation of the final products, where *cis*-transition structures show an eclipsed *pseudo*-twist/boat conformation, while

trans-counterparts present a *pseudo*-chair confirmation (Figure 3C).

Next, we examined the underlying factors leading to the computed *cis*:trans selectivity using the activation strain (ASM) – distortion/interaction analysis (Figure 4).[5,19,20] Additionally, we further decompose the interaction energy within the energy decomposition analysis framework (EDA,[21,24] Figure 5 and Table 2).

In all cases, at the initial stages of the reaction, the reaction profile goes up in energy due to the strain energy required to

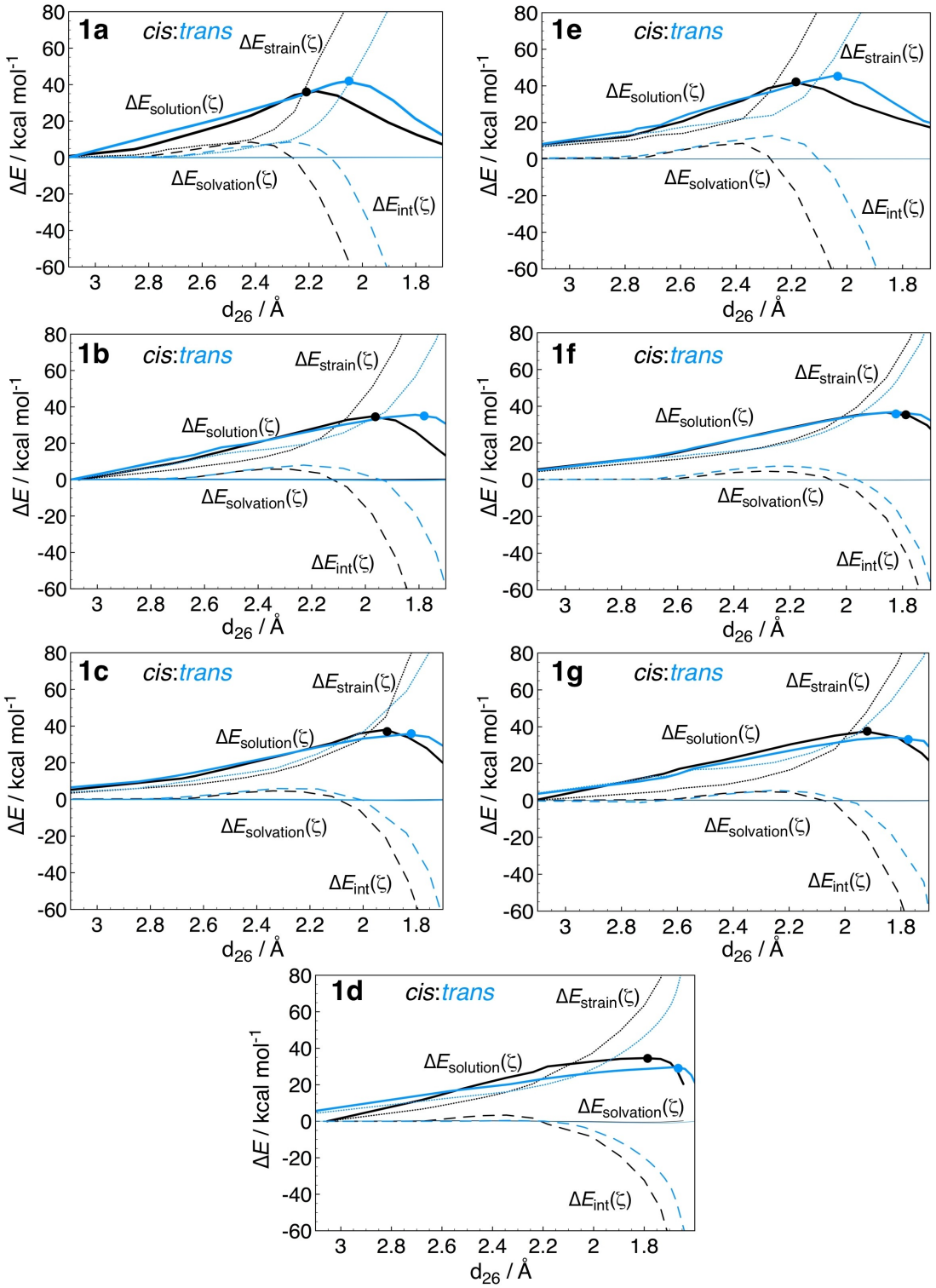

Figure 4. Activation strain analyses along the IRC projected the newly formed C–C bond (d_{26}) of **1a**–**g** intramolecular ene-Alder reaction computed at ZORA-M062X/TZVP level of theory. Transition state geometries are indicated with a dot.

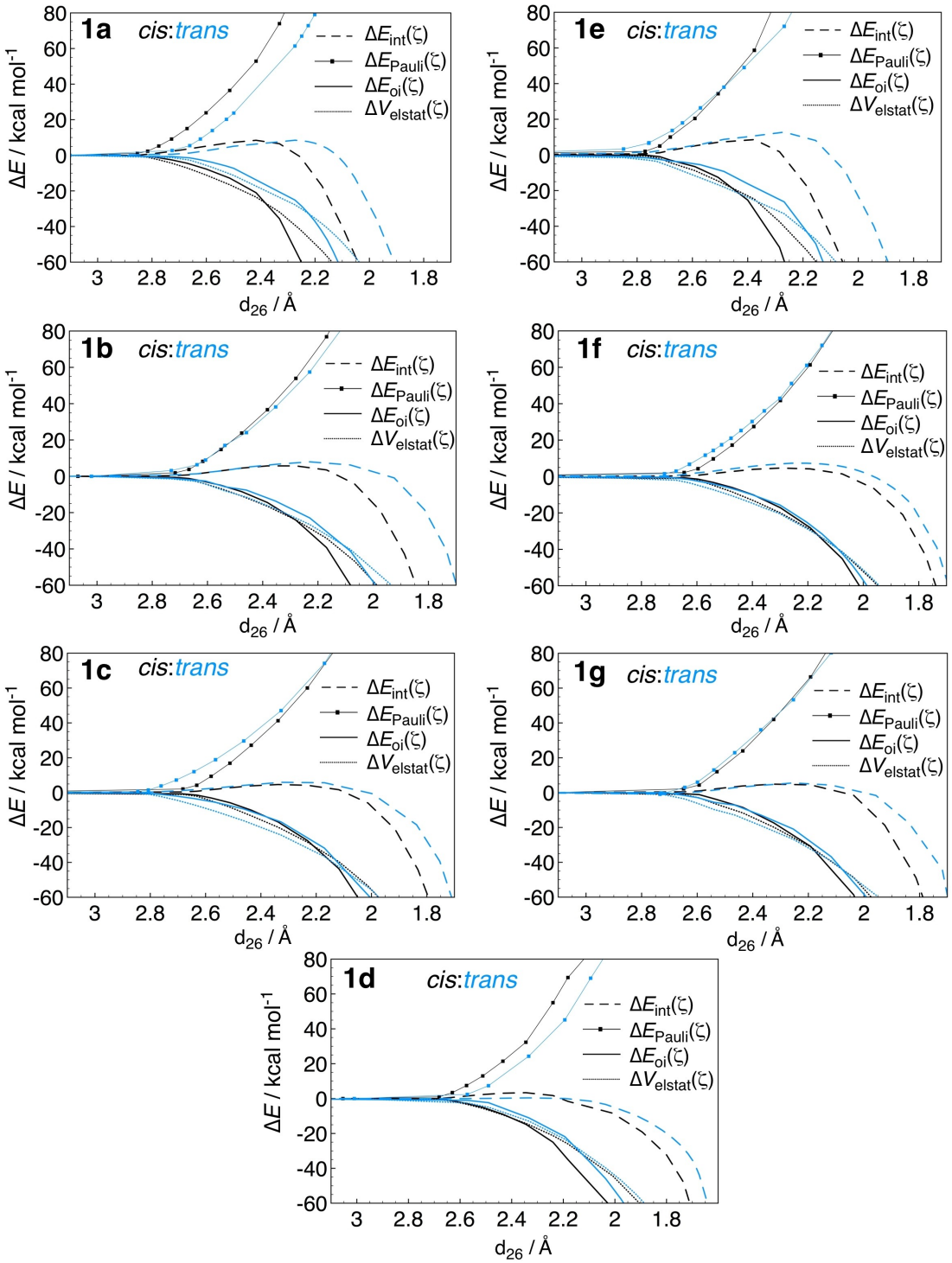

Figure 5. Energy decomposition analyses along the IRC projected the newly formed C–C bond (d_{26}) of **1a–g** intramolecular ene-Alder reaction computed at ZORA-M062X/TZVP level of theory.

deform the reagents and elongate the C8-Ha bond, plus the destabilizing interaction energy between ene-enophile moieties consequence of Pauli repulsion. As the reaction proceeds, in the vicinity of the transition structure geometry (when the newly formed C2–C6 and C1–Ha bonds begin to develop) the interaction curve starts becoming stabilizing. This situation has been already described for hetero ene-Alder reactions[3c] and other pericyclic reactions.[25] Remarkably, our calculations show that solvation has negligible effects on the reaction profiles, as shown by a flat solvation curve ($\Delta E_{solvation}$ in Figure 4).

Starting from the pattern structure **1a**, exclusive formation of *cis*-**2a** can be addressed to the existence of a *reactive-like*

Table 2. Energy decomposition analysis (EDA), strain energies (in kcal mol^{-1}) and $<HOMO_{ene} \mid LUMO_{enophile}>$ orbital overlap of transition structures associated with studied intramolecular ene-Alder reactions computed at M06-2X(PCM)/TZVP level.

entry		2	ΔE_{Pauli}	ΔV_{elstat}	ΔE_{oi}	ΔE_{strain}			$<HOMO_{ene} \mid LUMO_{enophile}>$
						[ene]	[enophile]	total	
1	**1 a**	*cis*	141.0	−58.1	−96.9	39.6	11.4	51.0	0.205
2		*trans*	131.7	−59.5	−83.2	36.2	16.9	53.1	0.228
3	**1 b**	*cis*	154.6	−67.8	−102.4	34.8	16.1	50.9	0.194
4		*trans*	181.2	−85.8	−115.6	32.9	23.6	56.5	0.222
5	**1 c**	*cis*	156.0	−71.3	−102.9	32.3	21.7	54.0	0.183
6		*trans*	180.0	−85.2	−111.1	32.6	26.4	59.0	0.203
7	**1 d**	*cis*	195.5	−85.8	−137.1	38.3	25.1	63.4	0.180
8		*trans*	240.2	−106.8	−173.3	38.4	32.4	70.9	0.195
9	**1 e**	*cis*	145.3	−62.5	−98.7	41.8	16.6	58.4	0.138
10		*trans*	143.9	−65.5	−86.8	36.5	17.9	54.4	0.222
11	**1 f**	*cis*	173.2	−81.1	−109.9	33.1	22.3	55.5	0.210
12		*trans*	187.2	−88.3	−115.7	32.4	22.2	54.6	0.223
13	**1 g**	*cis*	161.1	−65.0	−107.2	32.1	15.4	47.5	0.181
14		*trans*	184.4	−89.8	−112.8	28.8	21.8	53.6	0.202

transition structure **TSa**-*cis* in which the stabilizing interaction curve develops at long C2–C6 distances (d_{26} = 2.17 Å). Within this approach, the orbital and electrostatic interactions compensate the destabilizing Pauli repulsion and the strain energy at early stages of the reaction. On contrary, in highly asynchronous **TSa**-*trans*, the forming C2–C6 bond is more developed (d_{26} = 2.05 Å). Therefore, in the transition structure geometry, the stabilizing $HOMO_{ene}$–$LUMO_{enophile}$ orbital interaction engages at cost of higher deformation of the initial reagent, thus the activation barrier rises (total strain energy of +51.0 and +53.1 kcal mol^{-1} for **TSa**-*cis* and **TSa**-*trans*, respectively). However, some other factors such as a higher stabilizing orbital interaction that compensates a slightly higher Pauli repulsion in **TSa**-*cis* compared to **TSa**-*trans* also point towards the computed *cis*-specificity (entries 1–2 in Table 2).

The presence of activating groups reduce the activation barriers and strongly affects the *cis*:*trans* ratio, increasing *trans*-product formation. For instance, *E*-monosubstituted compound **1 b** (X=CO_2Me; Y=H in Scheme 1) changes the reaction from *cis*-specific (*vide supra*) to *cis*-selective, where *cis*-**2 b** formation is favored. On the other hand, *Z*-isomer **1 c** (X=H; Y=CO_2Me in Scheme 1) yields a mixture of *cis*-**2 c**: *trans*-**2 c** where formation of the latter is slightly favored. Additionally, the *trans*-preference is more clear for malonate derivative **2 d**, where *trans*-**2 d** is the major product.[8]

Remarkably, CO_2Me groups induce an increase in the asynchronicity on **TSb–d** geometries, where C2–C6 distances are reduced 0.2–0.4 Å compared to unsubstituted **TSa**. This effect is more pronounced in the *trans* approaches. We hypothesize that this fact is associated with a change in the shape of $LUMO_{enophile}$ that delocalizes on the C=O moiety of the electronwithdrawing group (Figure 6). Therefore higher C2–C6 proximity is required to engage stabilizing $<HOMO_{ene} \mid LUMO_{enophile}>$ interaction. Actually, activation strain (ASM) and energy decomposition analysis (EDA) show that the higher asynchronicity in the transition state of *trans* approaches is reflected in a more stabilizing orbital and electrostatic interaction compared to their *cis* counterparts. These interactions compensate the destabilizing Pauli repulsion and/or strain energy associated with a more developed C2–C6 bond, thus prompting *trans*-product formation.

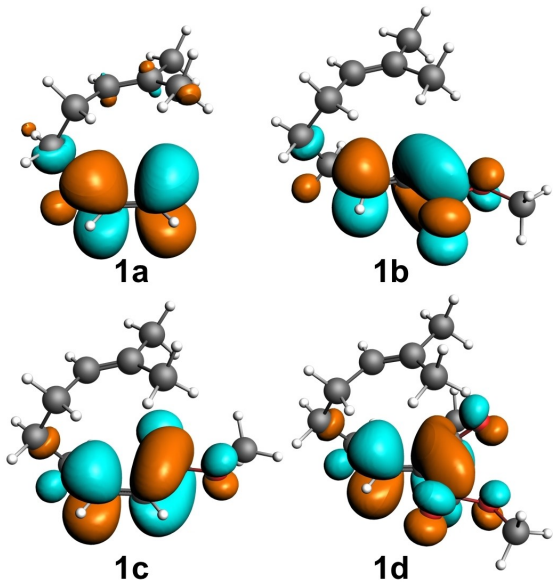

Figure 6. Plot of the LUMO (enophile) of compounds **1 a–d** at isosurface value = 0.035.

For **1 b**, we observe that *cis*-selectivity is associated with lower total strain energy compared to the *trans* analog, as found for **1 a**. Here, the presence of CO_2Me group implies an increase of stabilizing orbital and electrostatic interactions that slightly favor the *trans* reaction profile, thus reducing the energetic difference (0.8 kcal mol^{-1} activation Gibbs free energy difference between **TSb**-*cis* and **TSb**-*trans*, compared to the 2.8 kcal mol^{-1} difference computed for **1 a**). In this case, the CO_2Me group is placed in equatorial position in both *cis*- and *trans*-transition structures (Figure 3). Contrary to it, in **1 c** transition structures, the CO_2Me group is placed in axial position. Due to that, the **TSC**-*cis* *pseudo*-boat transition state geometry is deformed towards a *pseudo*-twist conformation to reduce the 1,3-diaxial interaction with the tether (dihedral angle

θ_{b26c} of 24° and 42° in **TSb**-*cis* and **TSC**-*cis*, respectively). However, **TSc**-*trans* pseudo-chair conformation is not affected, because the CO_2Me group is placed far away from the tether. In fact, the deformation observed on **TSC**-*cis* affects the $<HOMO_{ene} \mid LUMO_{enophile}>$ overlap, thus reducing the orbital interaction stabilization compared to **TSc**-*trans* counterparts (overlaps of 0.183 and 0.203, associated with orbital interaction of −102.4 and −115.6 kcal mol^{-1} for **TSC**-*cis* and **TSc**-*trans*, respectively).

In highly activated malonate derivatives **1 d** both transition structures are more asynchronous than the ones observed for **1 a**–**c**, as shown by a closer C2–C6 distances, and lower C8-Ha elongations. In **TS1d**-*trans*, the highest asynchronicity (as shown by the shortest C2–C6 distance) is related to an increase in the stabilizing orbital and electrostatic interactions[3c] that overcomes the rise in Pauli repulsion. On the other hand, the analogous rise in Pauli repulsion of **TS1d**-*cis* related to the asynchronicity increase (compared to **TS1a**-*cis*) is not compensated by the lower orbital or the electrostatic stabilization, due to the CO_2Me moiety in axial position.[26] Therefore, *trans*-selectivity is observed.

Next we analyzed the intramolecular Alder-ene reaction of methylated compounds **1 e**–**g** not reported in literature. Our results show that presence of methyl groups favors the formation *trans*-cyclopentanes, compared to non-methylated analogs **1 a**–**c**. In fact, to our surprise, the presence of two methyl groups (**1 e**) does not affect the transition structure geometries but affects the *cis*:*trans* ratio (96:4 vs 88:12 for **1 a** and **1 e**). In this latter case, the predicted *cis*-preference is consequence of an early transition structure in which the stabilizing interaction curve develops at long C2–C6 distances (*vide supra*). However, we note an increase in the total strain energy in **TSe**-*cis* that reduces the *cis*-preference compared to unsubstituted compound **1 a** (strain energy increase of 4.5 kcal mol^{-1} in **TSe**-*cis* and 1.5 kcal mol^{-1} in **TSe**-*trans*, considering **TSa** analogous as reference).

Finally, in heterodisubstituted compounds **1 f**–**g** we found that the formation of *trans*-products are more favored than in monosubstituted analogous **1 b**–**c** because in all TSs there is a group placed in *Z*-position (theoretical *cis*:*trans* ratios of 4:96 and 17:83 for **1 f** and **1 g** vs 66:34 and 25:75 for **1 b** and **1 c**). In these cases, the presence of a group in axial position of the *cis*-transition structures implies a deformation from the pattern *pseudo*-boat to a *pseudo*-twist conformation that destabilizes them, favoring *trans*-**2** formation (*vide supra*). Remarkably, that effect is more visible for **TSf**-*cis* where more sterically demanding group Me[27] is placed in axial position of the transition structure. Thus, showing a more distorted transition state geometry than **TSg**-*cis* analog (θ_{b26c} of 46° vs 40°, associated with total strain energy of 55.5 and 47.5 kcal mol^{-1} for **TSf**-*cis* and **TSg**-*cis*, respectively).

Conclusions

Intramolecular Alder-ene reaction of 1,6-dienes can proceed via six membered *pseudo*-boat *cis*- or *pseudo*-chair *trans*-asynchronous transition structures where the C2–C6 bond develops earlier than the breaking/forming C–H bonds.

For unactivated reagents observed *cis*-selectivity is related with lower strain energy, consequence of an early transition structure characterized by long C2–C6 distances.

The presence of activating groups reduces the activation barrier and increases the asynchronicity of the transition structure. In these cases the C2–C6 distances are closer compared to the pattern structure due to the modification in the LUMO of the enophile. Due to that, an increase of the Pauli repulsion and/or strain energy is observed in order to engage the stabilizing $<HOMO_{ene} \mid LUMO_{enophile}>$ orbital interaction. Remarkably, enhanced stabilizing orbital and electrostatic interaction in *trans* approaches overcomes this Pauli repulsion increase, thus favoring the formation of *trans*-products. Additional higher *trans*-preference is observed for *Z*-substituted 1,6-dienes due to 1,3-diaxial interaction that can distort the *cis*-**TS**, thus decreasing the orbital interaction stabilization. In these cases, we hypothesize that the reduction of stabilizing interactions in the *cis*-transition structures due to the *pseudo*-twist/boat conformation has similar impact on the intramolecular ene-Alder *cis*:*trans* ratio than the increase of stabilizing interactions in the *trans*-ones.

Additionally, our calculations predict the presence of Me groups on *Z*-position also increases the *trans*-selectivity.

Acknowledgements

SGI-IZO-SGIker (UPV/EHU) and DIPC are acknowledged for generous allocation of computational resources.

Conflict of Interest

There are no conflicts to declare.

Data Availability Statement

The data that support the findings of this study are available from the corresponding author upon reasonable request.

Keywords: intramolecular Alder-ene · DFT · selectivity · activation strain model · energy decomposition analysis

[1] K. Alder, F. Pascher, A. Schmitz, *Ber. Dtsch. Chem. Ges.* **1943**, *76*, 27–53.
[2] a) K. Mikami, M. Shimizu, *Chem. Rev.* **1992**, *92*, 1021–1050; b) A. Novikov, A. Zakarian, *Sigmatropic shifts and ene reactions (excluding [3,3])* in, *Applications of Domino Transformations in Organic Synthesis Volume 2*; Ed. S. A. Snyder; Thieme Chemistry, Stuttgart **2016**; c) P. Saha, A. K. Saikia, *Org. Biomol. Chem.* **2018**, *16*, 2820–2840; d) M. Ohasi, C. S. Jamieson Y Cai, D. Tan, D. Kanayama, M.-C. Tang, S. M. Anthony, J. V. Chari, J. S. Barber, E. Picazo, T. B. Kakule, S. Cao, N. K. Garg, J. Zhou, K. N. Houk, Y. Tang, *Nature* **2020**, *586*, 64–69.
[3] a) R. J. Loncharich, K. N. Houk, *J. Am. Chem. Soc.* **1987**, *109*, 6947–6952; b) G. D. Paderes, W. L. Jorgensen, *J. Org. Chem.* **1992**, *57*, 1904–1916; c) I. Fernández, F. M. Bickelhaupt, *J. Comp. Chem.* **2012**, *33*, 509–516;

d) R. Jin, S. Liu, Y. Lan, *RSC Adv.* **2015**, *5*, 61426–61435; e) E. H. Tiekink, P. Vermeeren, F. M. Bickelhaupt, T. A. Hamlin, *Eur. J. Org. Chem.* **2021**, 5275–5283.
[4] a) B. R. Woodward, R. Hoffmann, *The Conservation of Orbital Symmetry*; Academic Press: New York, **1969**; b) S. Inagaki, H. Fujimoto, K. Fukui, *J. Am. Chem. Soc.* **1976**, *98*, 4693–4701.
[5] a) P. Vermeeren, T. A. Hamlin, F. M. Bickelhaupt, *Chem. Commun.* **2021**, *57*, 5880–5896; b) F. M. Bickelhaupt, K. N. Houk, *Angew. Chem. Int. Ed.* **2017**, *56*, 100070–10086; c) L. P. Wolters, F. M. Bickelhaupt, *WIREs Comput. Mol. Sci.* **2015**, *5*, 324–343; d) I. Fernandez, F. M. Bickelhaupt, *Chem. Soc. Rev.* **2014**, *43*, 4953–4967; e) D. H. Ess, K. N. Houk, *J. Am. Chem. Soc.* **2007**, *129*, 10646–10647; f) F. M. Bickelhaupt, *J. Comput. Chem.* **1999**, *20*, 114–128.
[6] W. Oppolzer, V. Snieckus, *Angew. Chem. Int. Ed.* **1978**, *17*, 476–486.
[7] W. D. Huntsman, V. C. Solomon, D. Eros, *J. Am. Chem. Soc.* **1958**, *80*, 5455–5458.
[8] S. K. Ghosh, T. K. Sarkar, *Tetrahedron Lett.* **1986**, *27*, 525–528.
[9] M. Terada, *Ene Reactions* in *Science of Synthesis, Volume 3: Stereoselective Synthesis 3*. Ed. P. A. Evans, Thieme Verlagsgruppe, Stuttgart, **2011**.
[10] B. E. Thomas IV, R. J. Loncharich, K. N. Houk, *J. Org. Chem.* **1992**, *57*, 1354–1362.
[11] G. K. Das, *J. Chem. Soc., Perkin Trans. 2* **1999**, 1779–1782.
[12] a) N. Mondal, S. C. Mandal, G. K. Das, *J. Mol. Struct. (Theochem)* **2004**, *617*, 189–196; b) S. Roy, K. Chakrabarty, G. K. Das, *J. Mol. Struct. (Theochem)* **2007**, *820*, 112–117; c) K. Chakrabarty, S. Roy, S. N. Gupta, G. K. Das, *J. Mol. Struct. (Theochem)* **2009**, *901*, 44–48.
[13] R. G. Parr, W. Yang, *Density-Functional Theory of Atoms and Molecules*, Oxford, New York, **1989**.
[14] Gaussian16, Revision B.01, M. J. Frisch et al., Gaussian Inc., Wallingford CT, **2016** (full reference in the Supporting Information).
[15] AMS 2022.1, SCM, Theoretical Chemistry, Vrije Universiteit, Amsterdam, The Netherlands, **2021** (http://www.scm.com).
[16] a) Y. Zhao, D. G. Truhlar, *Acc. Chem. Res.* **2008**, *41*, 157–167; b) Y. Zhao, D. G. Truhlar, *Theor. Chem. Acc.* **2008**, *120*, 215–241.
[17] A. Schaefer, C. Huber, R. Ahlrichs, *J. Chem. Phys.* **1994**, *100*, 5829–35.
[18] R. Cammi, B. Mennucci, J. Tomasi, *J. Phys. Chem. A* **2000**, *104*, 5631–5637.
[19] J. Tomasi, B. Mennucci, R. Cammi, *Chem. Rev.* **2005**, *105*, 2999–3093.
[20] I. Fernández, F. M. Bickelhaupt, F. P. Cossío, *Chem. Eur. J.* **2014**, *20*, 10791–10801.
[21] a) J. Z. A. Laloo, L. Rhyman, P. Ramasami, F. M. Bickelhaupt, A. de Cózar, *Chem. Eur. J* **2016**, *22*, 4431–4439; b) J. Z. A. Laloo, L. Rhyman, O. Larrañaga, P. Ramasami, F. M. Bickelhaupt, A. de Cózar, *Chem. Asian J.* **2018**, *13*, 1138–1147.
[22] a) F. M. Bickelhaupt, E. J. Baerends, *Reviews in Computational Chemistry*, Vol. 15; K. B. Lipkowitz, D. B. Boyd, Eds.; Wiley-VCH: New York, **2000**, pp. 1–86; b) M. Lein, G. Frenking, *Theory and Applications of Computational Chemistry. The First 40 Years*; C. E. Dykstra, G. Frenking, K. S. Kim, G. E. Scuseria, Eds.; Elsevier: Amsterdam, **2005**.
[23] H. Eyring, M. Polanyi, *Z. Phys. Chem. B* **1931**, *12*, 279–311.
[24] For clarity, in EDA profiles (Figure 5) and in Table 2 ΔE_{Pauli}, ΔV_{elstat} and ΔE_{oi} are normalized to consider $\Delta E_{int} = 0$ for the reactive complexes.
[25] a) I. Fernandez, F. M. Bickelhaupt, F. P. Cossío, *Chem. Eur. J.* **2009**, *15*, 13022–13032; b) I. Fernandez, F. P. Cossío, F. M. Bickelhaupt, *J. Org. Chem.* **2011**, *76*, 2310–2314.
[26] Note that in this case, due to the presence of two CO_2Me groups the deformation of the pseudo-boat conformation is not required to engage the $HOMO_{ene}$–$LUMO_{enophile}$ orbital interaction.
[27] Steric hindrance values of 1.7 and 1.27 for Me and CO_2Me groups based on Gibbs energy differences between cyclohexane equatorial-axial conformations. See page 696 of E. L. Eliel, S. H. Wilen, L. N. Mander, *Stereochemistry of Organic Compounds*, Wiley, New York **1994**.

Manuscript received: June 2, 2022
Revised manuscript received: August 7, 2022
Accepted manuscript online: August 8, 2022
Version of record online: September 2, 2022